Available online at www.sciencedirect.com
SCIENCE DIRECT®
ELSEVIER
International Journal of Solids and Structures 43 (2006) 3675–3691
INTERNATIONAL JOURNAL OF SOLIDS and STRUCTURES
www.elsevier.com/locate/ijsolstr

Mechanical behavior of functionally graded material plates under transverse load—Part II: Numerical results

Shyang-Ho Chi [a,1], Yen-Ling Chung [b,*]

[a] First International Computer, Inc., 4FL, No. 300, Yang Guang St., NeiHu, Taipei, Taiwan, ROC
[b] Department of Construction Engineering, National Taiwan University of Science and Technology, P.O. Box 90-130, Taipei 10672, Taiwan, ROC

Received 4 April 2005
Available online 13 June 2005

Abstract

The formulations of the complete solutions to the rectangular simply supported plates with power-law, sigmoid, and exponential FGMs have been derived in Part I. In this part, we focus on the numerical solutions evaluated directly from theoretical formulations and calculated by finite element method using MARC program. The effects of loading conditions, the change of Poisson's ratio, and the aspect ratio on the mechanical behavior of an FGM plate are discussed. Besides, a comparison of the results of P-FGM, S-FGM, and E-FGM is investigated.

Keywords: Power-law FGM plate; Sigmoid FGM plate; Exponential FGM plate; Finite element method

1. Finite element models

In the numerical calculation, consider a square FGM plate with the ratio of width to thickness equal to 50, i.e., $a = b = 100$ cm, $h = 2$ cm. The plate is simply supported on its four sides and is subjected to the transverse load, as shown in Fig. 1. The Poisson's ratio of the FGM plate is assumed to be constant in the whole plate. Take $v = 0.3$. The Young's moduli at the top and bottom surfaces of the FGM plate are assumed to be E_2 and E_1, respectively. However, the Young's modulus at any point on the FGM plate varies continuously in the thickness direction based on the volume fraction of the constituents.

* Corresponding author. Tel.: +886 2 2737 6558; fax: +886 2 2737 6606.
E-mail addresses: sona@rd.fic.com.tw (S.-H. Chi), chung@hp.ct.ntust.edu.tw (Y.-L. Chung).
[1] Tel.: +886 2 8751 8751x6961; fax: +886 2 8751 8826.

0020-7683/$ - see front matter
doi:10.1016/j.ijsolstr.2005.04.010

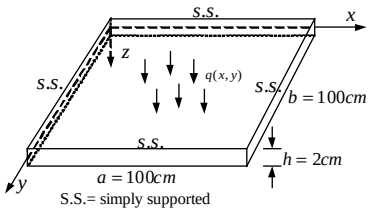

Fig. 1. The configuration of a simply supported rectangular FGM plate.

Due to the symmetry about the x- and y-axes, only one quarter of the full plate is under consideration when using the finite element program MARC. In the finite element mesh, 16 layers in the thickness direction are used to simulate the variation of the material properties of the FGM plate. Each layer has constant material properties, but the material properties differ from layer to layer. The material properties of all layers in the mesh are determined from the functions of volume fractions in Part I, according to the given E_1, E_2 and v. Moreover, because there is no any stress singularities in the plate, solid eight-node elements are used.

2. The S-FGM plates

The material properties of S-FGM plates vary continuously and functionally based on the volume fraction of the sigmoid distribution, given in Eq. (4) of Part I of this paper. It is assumed that the Young's modulus at the bottom surface of the S-FGM plate, E_1, is 2.1×10^6 Kg/cm^2, while that at the top surface of the S-FGM plate, E_2, varies with the ratio of E_1/E_2. The variations of Young's modulus of the S-FGM plate versus the ratio of E_1/E_2 are plotted in Fig. 2 for the case of the material exponent $p = 2$.

The series solution to the S-FGM plate with material property of $E = E(z)$ only is given in Eq. (46) of Part I. Now, consider the special case that the material exponent $p = 2$. Then the quantities of S_{11} and Q_{11} in Eq. (48) of Part I for the case of $p = 2$ can be simplified as

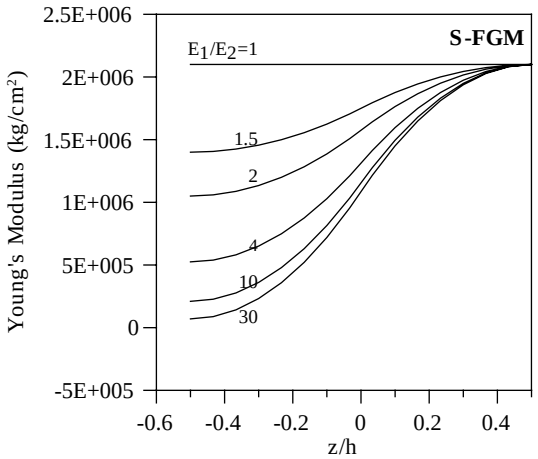

Fig. 2. The variation of the Young's moduli of an S-FGM plate for different ratio of E_1/E_2.

$$S_{11} = \frac{h^3 E_2}{8(1-\nu^2)}\left[\frac{E_1/E_2+1}{3} - \frac{25(E_1/E_2-1)^2}{144(E_1/E_2+1)}\right] \tag{1}$$

$$Q_{11} = -\frac{5h(E_1/E_2-1)}{24(E_1/E_2+1)} \tag{2}$$

2.1. Under uniform load

First, consider that the S-FGM plate is subjected to a uniform load with the magnitude $q_0 = 1$ Kg/cm^2. Expanding the uniform load into a Fourier series, we obtain

$$q_z(x,y) = q_0 = \sum\sum q_{mn} \sin\frac{m\pi x}{a} \sin\frac{n\pi y}{b} \tag{3a}$$

The coefficient q_{mn} can be evaluated by Eq. (19) of Part I and is

$$q_{mn} = \frac{16q_0}{\pi^2 mn} \quad m,n = 1,3,5,\ldots \tag{3b}$$

Consequently, the deflection, strain, and stress of the S-FGM plate under uniform load q_0 for $p = 2$ are evaluated by Eqs. (46) in Part I as

$$w = \frac{16q_0 b^4}{\pi^6}\cdot\frac{1}{S_{11}}\sum_m\sum_n \frac{1}{mn\left[\left(\frac{mb}{a}\right)^2+n^2\right]^2}\sin\frac{m\pi x}{a}\sin\frac{n\pi y}{b} \tag{4a}$$

$$\varepsilon_{xx} = \frac{16q_0 b^2}{\pi^4}\cdot\frac{(Q_{11}+z)}{S_{11}}\sum_m\sum_n \frac{\left(\frac{mb}{a}\right)^2}{mn\left[\left(\frac{mb}{a}\right)^2+n^2\right]^2}\sin\frac{m\pi x}{a}\sin\frac{n\pi y}{b} \tag{4b}$$

$$\sigma_{xx} = \frac{16q_0 b^2}{\pi^4}\cdot\frac{E(z)(Q_{11}+z)}{(1-\nu^2)S_{11}}\sum_m\sum_n \frac{\left(\frac{mb}{a}\right)^2+\nu n^2}{mn\left[\left(\frac{mb}{a}\right)^2+n^2\right]^2}\sin\frac{m\pi x}{a}\sin\frac{n\pi y}{b} \tag{4c}$$

$$\sigma_{yy} = \frac{16q_0 b^2}{\pi^4}\cdot\frac{E(z)(Q_{11}+z)}{(1-\nu^2)S_{11}}\sum_m\sum_n \frac{n^2+\nu\left(\frac{mb}{a}\right)^2}{mn\left[\left(\frac{mb}{a}\right)^2+n^2\right]^2}\sin\frac{m\pi x}{a}\sin\frac{n\pi y}{b} \tag{4d}$$

where the quantities of S_{11} and Q_{11} are given in Eqs. (1) and (2) of Part II.

For a square plate ($a = b$), the expressions of the deflection w, strain ε_{xx}, and stress σ_{xx} in Eqs. (4) involve the terms of $\frac{1}{mn(m^2+n^2)^2}$, $\frac{m}{n(m^2+n^2)^2}$, $\frac{m^2+\nu n^2}{mn(m^2+n^2)^2}$ respectively, which are independent of the material properties. Therefore, the convergence of $\sum_m\sum_n \frac{1}{mn(m^2+n^2)^2}$, $\sum_m\sum_n \frac{m}{n(m^2+n^2)^2}$, and $\sum_m\sum_n \frac{m^2+\nu n^2}{mn(m^2+n^2)^2}$ can be checked by comparing the series solutions corresponding to certain m and n terms of an isotropic homogeneous square plate with the finite element solution. It is found that for m and n greater than 12, the deflection, strain, and stresses of the series solutions will converge to constant values with errors less than 0.5%.

Hence, by applying $E_1 = 2.1\times10^6$ Kg/cm^2, $a = b = 100$ cm, $h = 2$ cm, $\nu = 0.3$, $q_0 = 1$ Kg/cm^2, $m = n = 20$ into Eqs. (4), the theoretical results can be evaluated without any difficulty. In addition, the plate problem is also investigated by finite element method. The theoretical and FEM results for the deflection w, strain ε_{xx}, and stress σ_{xx} are plotted in Figs. 3–5, respectively.

Fig. 3 shows that (i) the more E_1/E_2, the larger deflection w, because of the less stiffness of the FGM plate for larger E_1/E_2; (ii) the deflection of the FGM plate for $E_1/E_2 = 30$ is about five times of the homogeneous plate ($E_1/E_2 = 1$); (iii) the theoretical and numerical results agree very well with the maximum error less than 5%.

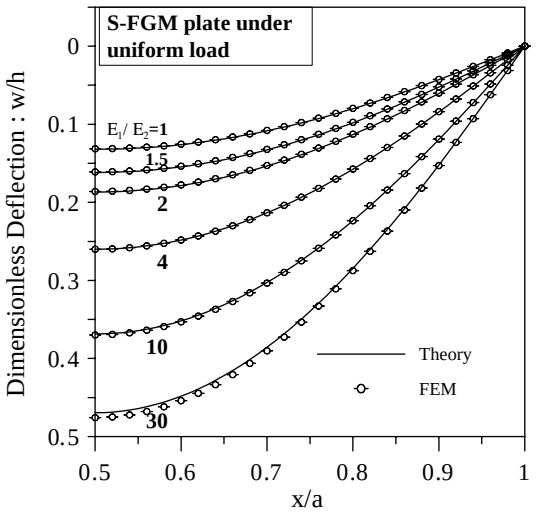

Fig. 3. The deflection of an S-FGM plate along the x direction for different E_1/E_2.

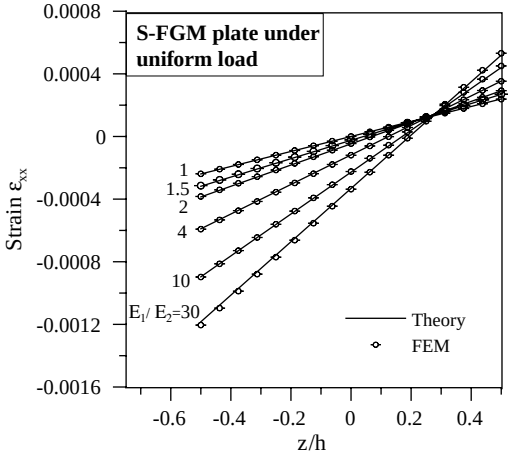

Fig. 4. The strain ε_{xx} at the center of an S-FGM plate for different E_1/E_2.

Fig. 4 represents the strain ε_{xx} at the center of the square plate ($x = a/2$, $y = a/2$) along the thickness direction. The strain ε_{xx} of the FGM plate calculated by FEM is linear, which supports the assumption that the strain is proportional to z. It is observed that the strain exists at the mid-surface ($z = 0$) of the FGM plate and it increases upon increasing E_1/E_2. It is well known that the neutral surface of a homogeneous plate is located at the mid-surface. However, for the FGM plate, Fig. 4 shows that the neutral surface moves to the positive z direction as the value of E_1/E_2 increases. The locations of the neutral surface of the S-FGM plate for different E_1/E_2 obtained from Fig. 4 are listed in Table 1. The maximum strain at the center of the FGM plate is compression and at the upper edge ($z = -h/2$).

The variation of the stress σ_{xx} at the center of the FGM plate along the thickness direction is depicted in Fig. 5. The stress of an S-FGM plate can be represented as a function of z of order 3, which is quite obvious for the case with $E_1/E_2 = 30$. This phenomenon coincides with the theoretical formulation in Eq. (4c), in

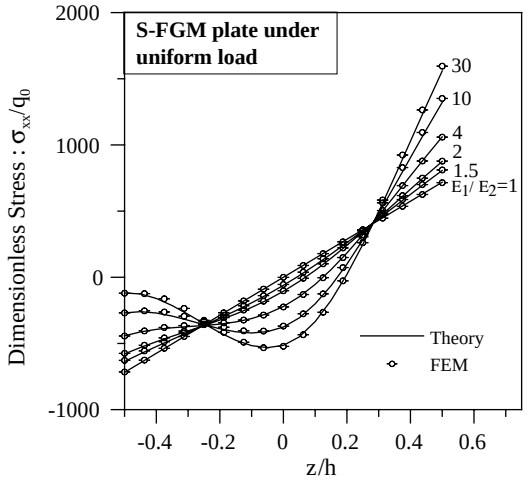

Fig. 5. The stress σ_{xx} at the center of an S-FGM plate for different E_1/E_2.

Table 1
The locations of the neutral surface of an S-FGM plate for different E_1/E_2

E_1/E_2	1	1.5	2	4	10	30
Location of the neutral surface (z/h)	0	0.04167	0.06945	0.125	0.17045	0.19489

which the stresses are proportional to $z \cdot E(z)$. In this section, the material parameter p is assumed to be 2, therefore the Young's modulus $E(z)$ is a function of z of order 2 and consequently the stress is a function of z of order 3.

The maximum tensile stress in the center of the S-FGM plate is at the bottom edge ($z = h/2$) and increases as the ratio E_1/E_2 increases. However, the maximum compressive stress is at the top surface ($z = -h/2$) for small E_1/E_2. As the ratio of E_1/E_2 increases, the maximum compressive stress moves to inside of the plate. The maximum compressive stress of the S-FGM can be obtained by differentiating the formation of stress in Eq. (4c) with respect to z. For the ratio $E_1/E_2 = 1$ in which the FGM plate becomes a homogeneous plate, the stress distribution is a linear function of z and the maximum stress is at the top or bottom surface of the plate.

2.1.1. The effect of the aspect ratio a/b

So far, the problem shown in Fig. 1 is assumed to be a square plate. However, it is worthwhile to investigate the effect of the aspect ratio a/b on the mechanical behavior of FGM plates. Therefore, in this section, all discussion are based on the assumption that a is fixed to be 100 cm and b is varying to investigate the effects of the aspect ratio a/b. The maximum deflection of the FGM plate shown in Fig. 1 is located at the center of the plate ($x = a/2$, $y = b/2$), and it is found from Eq. (4a) in the form of

$$w_{\max} = w(a/2, b/2) = \frac{16q_0b^4}{\pi^6} \cdot \frac{1}{S_{11}} \sum_m \sum_n \frac{1}{mn\left[\left(\frac{mb}{a}\right)^2 + n^2\right]^2} \tag{5}$$

The relation between the maximum deflection $w_{\max}$ and the aspect ratio a/b for different E_1/E_2 ratios is illustrated in Fig. 6. The maximum deflection $w_{\max}$ increases upon increasing the aspect ratio for a/b less

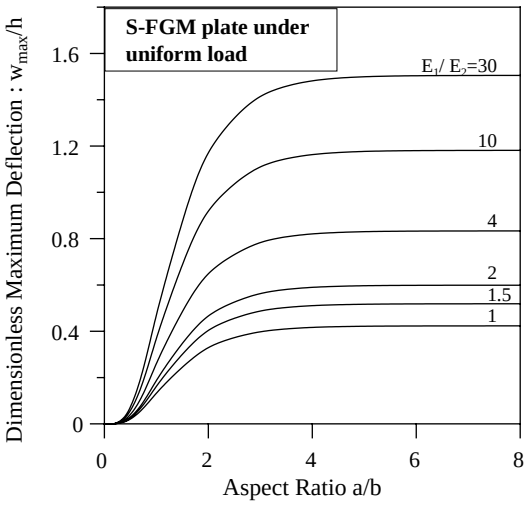

Fig. 6. The maximum deflection of an S-FGM plate versus the aspect ratio a/b for different E_1/E_2 ($a = 100$ cm, b is varying).

than 3. However, when a/b is greater than 3, the maximum deflection $w_{\max}$ of the rectangular FGM plate becomes a constant values. The strain and stress at the center of the plate are

$$\varepsilon_{xx}(a/2, b/2) = \frac{16q_0b^2}{\pi^4} \cdot \frac{(Q_{11} + z)}{S_{11}} \sum_m \sum_n \frac{\left(\frac{mb}{a}\right)^2}{mn\left[\left(\frac{mb}{a}\right)^2 + n^2\right]^2} \tag{6}$$

$$\sigma_{xx}(a/2, b/2) = \frac{16q_0b^4}{\pi^4} \cdot \frac{E(z)(Q_{11} + z)}{(1 - \nu^2)S_{11}} \sum_m \sum_n \frac{\left(\frac{mb}{a}\right)^2 + \nu n^2}{mn\left[\left(\frac{mb}{a}\right)^2 + n^2\right]^2} \tag{7}$$

For the case with $E_1/E_2 = 10$, the effects of the aspect ratio a/b on the strains ε_{xx}, ε_{yy} and stresses σ_{xx}, σ_{yy} at the center of the FGM plate are demonstrated in Figs. 7–10, respectively. It is observed that the neutral

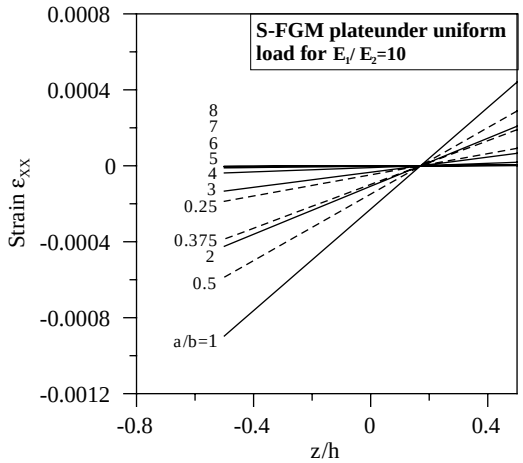

Fig. 7. The variation of the strain ε_{xx} at the center of an S-FGM plate for different aspect ratio a/b for a fixed as 100 cm and b varying.

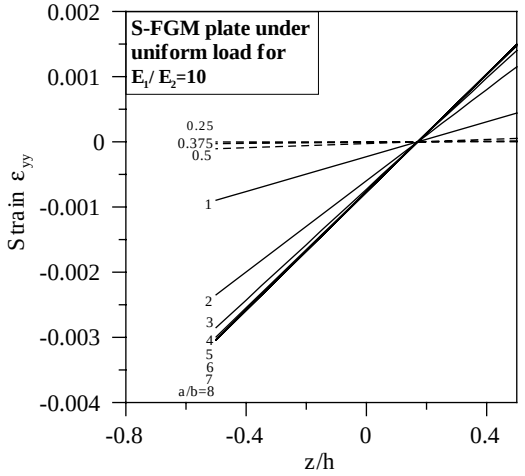

Fig. 8. The variation of the strain ε_{yy} at the center of an S-FGM plate for different aspect ratio a/b for a fixed as 100 cm and b varying.

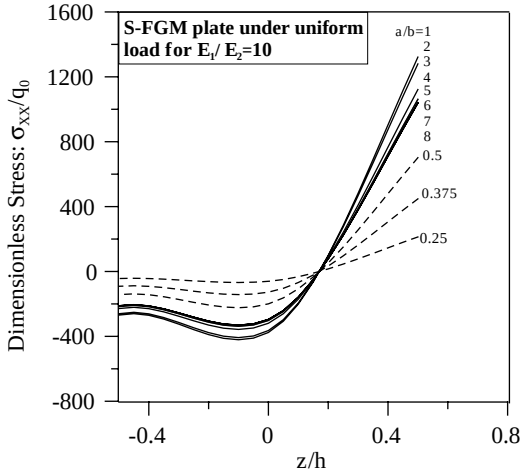

Fig. 9. The distribution of the stress σ_{xx} at the center of an S-FGM plate for different aspect ratio a/b for a fixed as 100 cm and b varying.

surfaces of the S-FGM plates for $E_1/E_2 = 10$ are at the same location, $z = 0.17h$, for a different aspect ratio a/b. Moreover, at the center of the FGM plate, the maximum strain located at the top surface of the plate ($z = -h/2$) increases with the increase of the aspect ratio a/b for $a/b < 1$, but decreases with the increase of the aspect ratio for $a/b > 1$.

At the center of the FGM plate, the maximum stress is tensile and is located at the bottom surface of the plate. To further understand the effect of the aspect ratio on the strain and stress, the maximum strains $(\varepsilon_{xx})_{\max}$, $(\varepsilon_{yy})_{\max}$ and stresses $(\sigma_{xx})_{\max}$, $(\sigma_{yy})_{\max}$ at the center of the plate versus the aspect ratio with different ratios of E_1/E_2 are plotted in Figs. 11–14, respectively. The maximum strain $(\varepsilon_{xx})_{\max}$ at the center of the plate vanishes when $a/b > 5$. However, the maximum strain $(\varepsilon_{yy})_{\max}$, and the maximum stresses $(\sigma_{xx})_{\max}$ and $(\sigma_{yy})_{\max}$ at the center of the plate remain constant when $a/b > 5$.

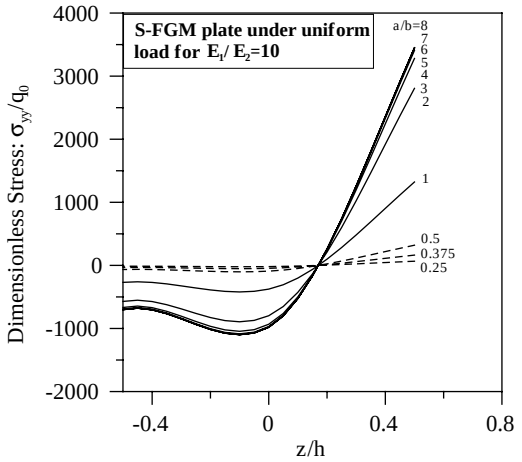

Fig. 10. The distribution of the stress σ_{yy} at the center of an S-FGM plate for different aspect ratio a/b for a fixed as 100 cm and b varying.

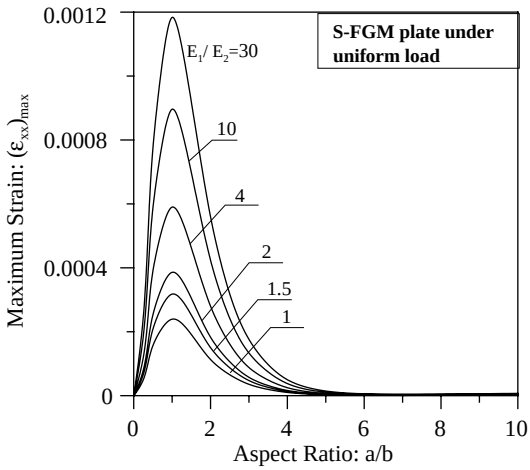

Fig. 11. The maximum strain $(\varepsilon_{xx})_{\max}$ at the center of an S-FGM plate versus the aspect ratio a/b for different E_1/E_2 ($a = 100$ cm, b is varying).

It is worthwhile to investigate whether the medium-thick plate assumption will hold for the FGM plates with different b/h ratio under certain aspect ratio a/b, especially for the case of large a/b values. To do this, consider an S-FGM rectangular plate with $E_1/E_2 = 10$ and Poisson's ratio $v = 0.3$ subjected to uniform load. The length of the plate a is fixed and taken as 100 cm. The width of the plate b is varying such that the aspect ratio $a/b = 1, 2, 4, 8, 9, 10$. For each aspect ratio a/b, change the thickness h so that the b/h value is in the range 5–25. The a/b values corresponding to different a/b and b/h ratios are listed in Table 2, in which the bold entries indicate that the thickness satisfies the medium-thick plate assumption, i.e., $a/h = 20$–100 approximately.

The maximum deflections $w_{\max}$ and the maximum tensile stresses $(\sigma_{xx})_{\max}$ at the center of the plates for different a/b and b/h ratios are estimated by both the theoretical formulae and finite element analysis.

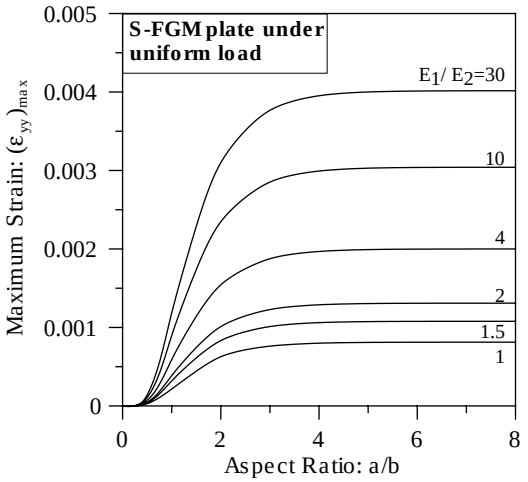

Fig. 12. The maximum strain $(\varepsilon_{yy})_{\max}$ at the center of an S-FGM plate versus the aspect ratio a/b for different E_1/E_2 ($a = 100$ cm, b is varying).

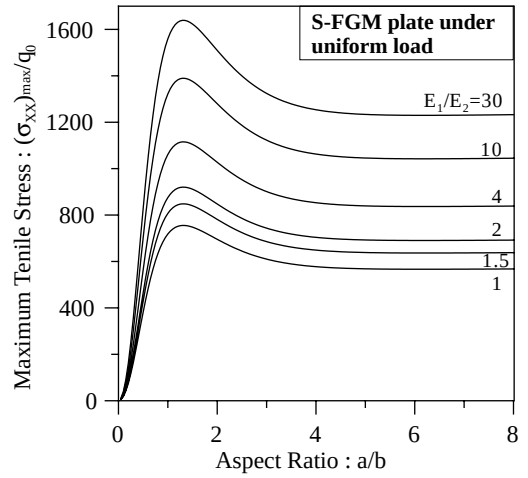

Fig. 13. The maximum tensile stress $(\sigma_{xx})_{\max}$ at the center of an S-FGM plate versus the aspect ratio a/b for different E_1/E_2 ($a = 100$ cm, b is varying).

Consequently the errors of the theoretical results compared with the finite element analysis are obtained. The errors of the maximum deflections $w_{\max}$ and maximum tensile stresses $(\sigma_{xx})_{\max}$ versus the b/h values for different aspect ratio a/b are shown in Figs. 15 and 16.

It is found from Figs. 15 and 16 that the errors of maximum deflections decrease as a/b value increases, so do the errors of the maximum tensile stresses when a/b increases to 4, whereas the errors increase slightly for $a/b = 8$, 9, 10. The reason might be because for certain b/h value, the smaller a/b has the thicker thickness h for which if the thickness does not fit the medium-thick plate assumption, the ignored transverse shear strain causes bigger errors. For the case $a/b = 4$, the thicknesses for $b/h = 5$–25 all satisfy the medium-thick plate assumption, i.e.,$a/h = 20$–100, and hence the error of the maximum tensile stress $(\sigma_{xx})_{\max}$

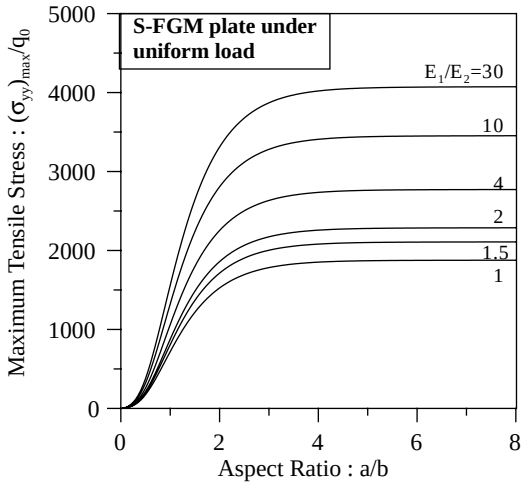

Fig. 14. The maximum tensile stress $(\sigma_{yy})_{max}$ at the center of an S-FGM plate versus the aspect ratio a/b for different E_1/E_2 ($a = 100$ cm, b is varying).

Table 2
The values of the ratio of a/h for different a/b and b/h ratios (a is fixed and taken as 100 cm)

	$a/b = 1$	$a/b = 2$	$a/b = 4$	$a/b = 8$	$a/b = 9$	$a/b = 10$
$b/h = 5$	5	10	**20**	**40**	**45**	**50**
$b/h = 6.25$	6.25	12.5	**25**	**50**	**56.25**	**62.5**
$b/h = 8.33$	8.33	16.7	**33.4**	**66.8**	**74.97**	**83.3**
$b/h = 12.5$	12.5	**25**	**50**	**100**	112.5	125
$b/h = 16.7$	16.7	**33.4**	**66.8**	133.6	150.3	167
$b/h = 20$	**20**	**40**	**80**	160	180	200
$Fb/h = 25$	**25**	**50**	**100**	200	225	250

The bold entries indicate that the value of a/h is in the range of medium-thick plate assumption ($a/h = 20$–100).

for $a/b = 4$ is the minimum in all different aspect ratios. However, the maximum deflection w_{max} behaves slightly different from the maximum tensile stress $(\sigma_{xx})_{max}$: the errors of the maximum deflections for $a/b = 4$ is not the minimum in all a/b values. When the aspect ratio a/b becomes larger, e.g., $a/b = 8$, 9, 10, the thickness satisfy the medium-thick plate assumption only for small values of b/h (see Table 2). Hence, the error of the maximum tensile stress $(\sigma_{xx})_{max}$ is small for small b/h but slightly increases for large b/h. However, the error of maximum deflection w_{max} shown in Fig. 15 presents the opposite behavior: the bigger b/h the small error even though the thickness is too thin to fit the medium-thick plate assumption.

Based on the above discussion, because the maximum deflections and maximum tensile stresses exhibit slightly different error behaviors, it seems that the b/h value which changes according to different aspect ratio a/b for certain thickness h does not significant affect the validness of the analytical solution based on the medium-thick plate assumption. Indeed, it can be simply concluded that if the FGM plate is too thick for which a/b and b/h are small, the transverse shear strain can not be ignored, and therefore the error of the analytical solution is big. If the thickness of the FGM plate fits the medium-thick plate assumption, even though the b/h value is not in the range of 20–100, the analytical results are valid within accept error. For the case of thin plates, for which a/b and b/h are big, although the FGM plates may be too thin to fit

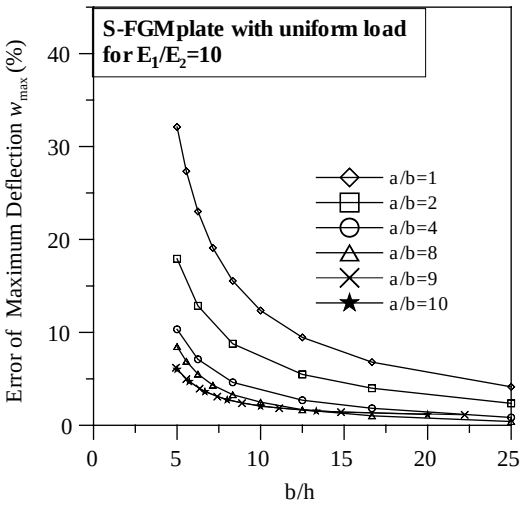

Fig. 15. The errors of the maximum deflection $w_{\max}$ at the center of an S-FGM plate versus the ratio b/h for different aspect ratio a/b in which a is taken as 100 cm and b is varying.

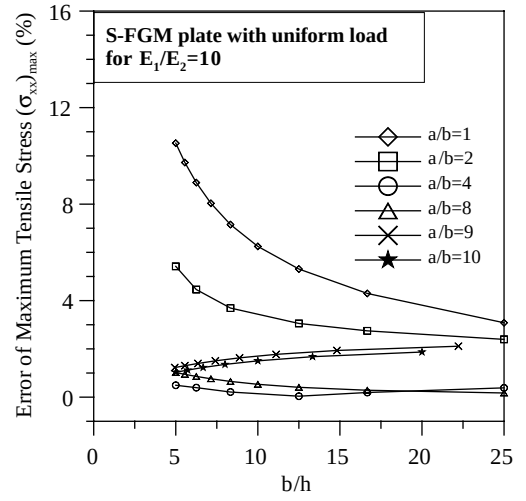

Fig. 16. The errors of the maximum tensile stress $(\sigma_{xx})_{\max}$ at the center of an S-FGM plate versus the ratio b/h for different aspect ratio a/b in which a is taken as 100 cm and b is varying.

the medium-thick plate assumption ($a/h = 20$–100 approximately), the theoretical solution based on the medium-thick plate assumption is also applicable with the errors less than 5%.

2.1.2. The effect of changing Poisson's ratio

The derivation of the theoretical result of the FGM plate in Part I is based on the assumption that the effects of changing Poisson's ratio can be neglected. Therefore, the Poisson's ratio v is assumed to be

constant in the theoretical solutions concerning the FGM plate. In this section, the effect of Poisson's ratio will be investigated by finite element analysis.

First, the S-FGM plate with $a = b = 100$ cm is considered, which is subjected to a uniform load, with the material properties of $E_1/E_2 = 10$ and a constant Poisson's ratio. To investigate the influence of Poisson's ratio, $v = 0.2$, 0.3 and 0.4 are considered. The deflection, strain, and stress of the S-FGM plate are illustrated in Figs. 17–19, in which the results of $v = 0.2$ and 0.4 are slightly different from that of $v = 0.3$.

Next, the same S-FGM plate is considered. However, the Poisson's ratio of the S-FGM plate is not a constant, but changes continuously with sigmoid distribution:

$$v(z) = g_1(z)v_1 + (1 - g_1(z))v_2 \quad \text{for } 0 < z < h/2 \tag{8a}$$

$$v(z) = g_2(z)v_1 + (1 - g_2(z))v_2 \quad \text{for } -h/2 < z < 0 \tag{8b}$$

where v_1 and v_2 are the Poisson's ratios at the lower and upper surfaces of the S-FGM plate. Here take $v_1 = 0.3$, $v_2 = 0.499$. The volume fractions $g_1(z)$ and $g_2(z)$ are defined in Eq. (3) of Part I.

For the case that $E_1/E_2 = 10$, $v_1 = 0.3$, $v_2 = 0.499$, $a = b = 100$ cm $h = 2$ cm, and $p = 2$, the deflection, strain, and stress of the S-FGM plates with functionally graded Poisson's ratios are plotted in Figs. 17–19. These figures show that the results of S-FGM plates with a constant Poisson's ratio ($v = 0.3$) and functionally graded Poisson's ratios are almost the same. This phenomenon implies that the influence of Poisson's ratio on the FGM plates can be neglected.

2.2. The comparison of the results under uniform, line, and point loads

To investigate the influence of an external load on the S-FGM plates, a square S-FGM plate under a line load with the magnitude $P_0 = 100$ Kg/cm at $x = a/2$ is considered such that the total load acting on the plate is equal to that of the uniform load with the magnitude $q_0 = 1$ Kg/cm^2. Then the coefficient q_{mn} at the Fourier expansion of the line load P_0 can be found from Eq. (31) of Part I as

$$q_{mn} = \frac{8P_0}{a\pi n} \sin\frac{m\pi}{2} \quad m, n = 1, 3, 5, \ldots \tag{9}$$

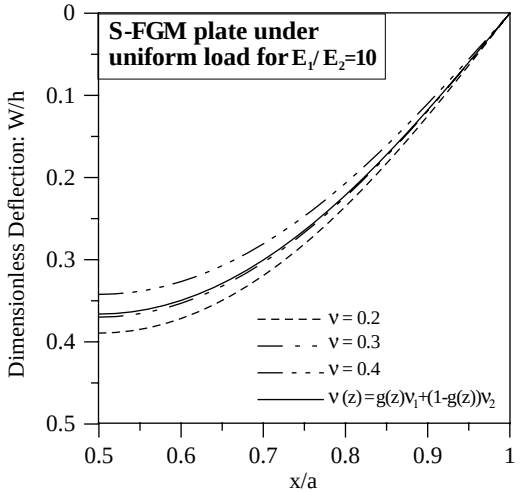

Fig. 17. The effects of Poisson's ratio on the deflection of an S-FGM plate for $E_1/E_2 = 10$.

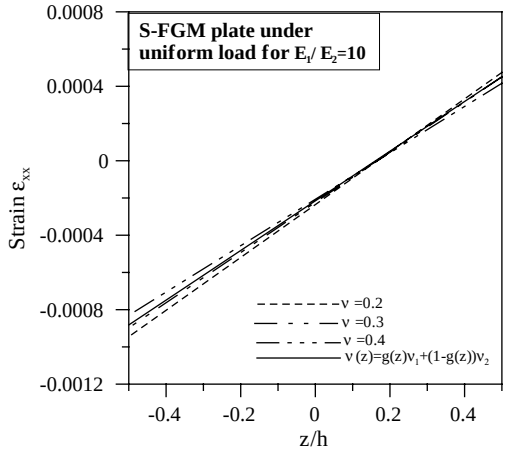

Fig. 18. The effects of Poisson's ratio on the strain ε_{xx} of an S-FGM plate for $E_1/E_2 = 10$.

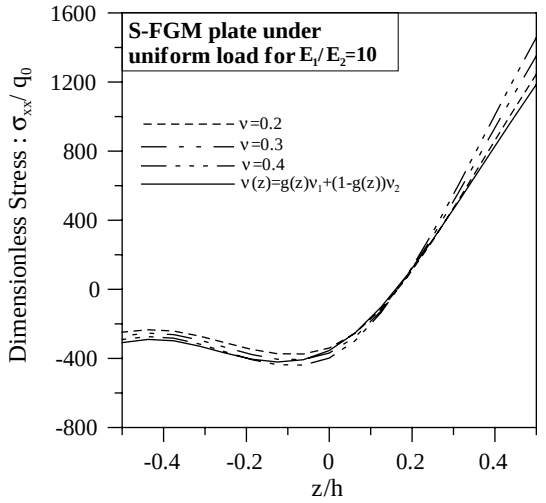

Fig. 19. The effects of Poisson's ratio on the stress σ_{xx} of an S-FGM plate for $E_1/E_2 = 10$.

In a manner similar to the line load, the S-FGM plate is assumed under a point load at the center of the plate with the magnitude $P = 10{,}000$ Kg, in which the total load is equal to that of the uniform load of $q_0 = 1$ Kg/cm^2. The coefficient q_{mn} at the Fourier expansion of the point load is found to be

$$q_{mn} = \frac{4P}{ab} \sin\frac{m\pi}{2} \sin\frac{n\pi}{2} \quad m, n = 1, 3, 5, \ldots \tag{10}$$

The deflection, strain, and stress of the S-FGM plate under line load P_0 and point load P can be evaluated by Eq. (46) of Part I without difficulty. The comparisons of the S-FGM plates under uniform, line, and point loads for $E_1/E_2 = 10$ are depicted in Figs. 20–22. It is shown in Fig. 21 that the three curves corresponding to uniform, line, and point loads intersect at the point of $z = 0.17h$, where is the location of the neutral surface of the S-FGM plate. Consequently, the location of the neutral surface is dependent on the material properties, but independent on the loading type.

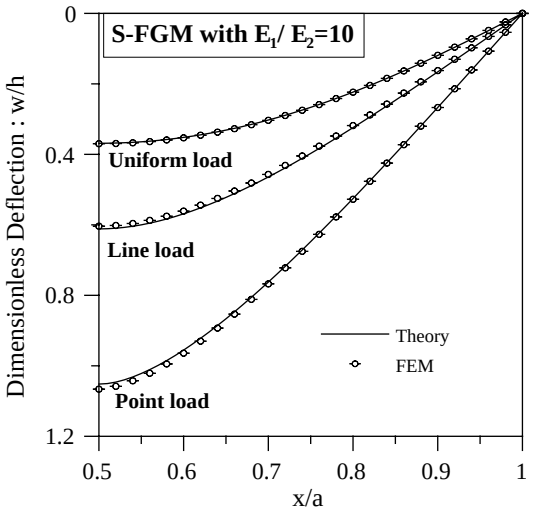

Fig. 20. The deflections of an S-FGM plate under uniform load, line load, or point load.

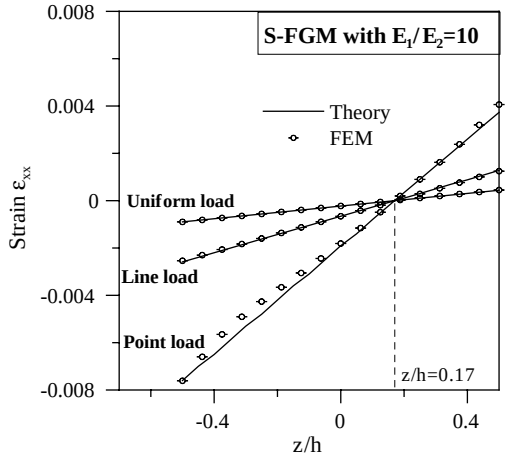

Fig. 21. The strains ε_{xx} at the center of an S-FGM plate under uniform load, line load, or point load.

3. The comparison of S-, P- and E-FGM plates

In this section, the problem in Fig. 1 is also under consideration. However, the Young's moduli of the FGM plates obeying the power-law or exponential functions (P-FGM or E-FGM plates), will be investigated and further compared with the results of S-FGM plates. The variations of the Young's moduli in the thickness direction for the P-FGM plate of $p = 2$ and $p = 0.5$ as well as the E-FGM plate for different E_1/E_2 are shown in Figs. 2 and 4 of Part I. The notations of $P_{0.5}$-FGM and P_2-FGM in Figs. 23–25 indicate the P-FGM plate for $p = 0.5$ and $p = 2$, respectively. It is observed from Figs. 2 and 4 of Part I that the stiffness of the $P_{0.5}$-FGM plate is stronger than that of S-FGM plate which is stronger than that of E-FGM plate. The P_2-FGM plate has the lowest stiffness.

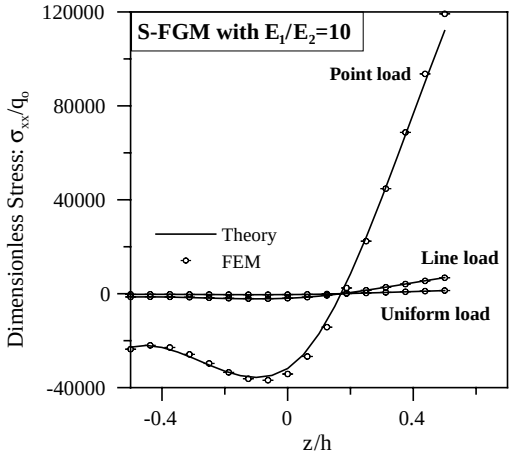

Fig. 22. The stresses σ_{xx} at the center of an S-FGM plate under uniform load, line load, or point load.

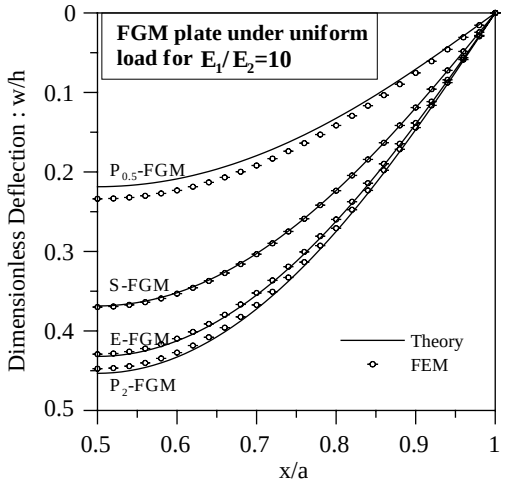

Fig. 23. The comparison of the deflections of $P_{0.5}$-FGM, S-FGM, E-FGM, and P_2-FGM plates for $E_1/E_2 = 10$.

Figs. 23–25 depict the deflections, strains and stresses at the center of $P_{0.5}$-FGM, S-FGM, E-FGM, and P_2-FGM plates subjected to uniform loads for $E_1/E_2 = 10$. It seems that the theoretical results of the S-FGM, E-FGM, and P_2-FGM agree very well with the finite element results. However, for the $P_{0.5}$-FGM plate, the theoretical and finite element results are slightly different. This is because the Young's modulus of the $P_{0.5}$-FGM varies rapidly near the upper surface of the plate and hence it is difficult to describe the material properties by finite element meshes. Moreover, the $P_{0.5}$-FGM plate which is stiffer than the other FGM plates has the smallest deflection, strain and stress among the four kinds of plates.

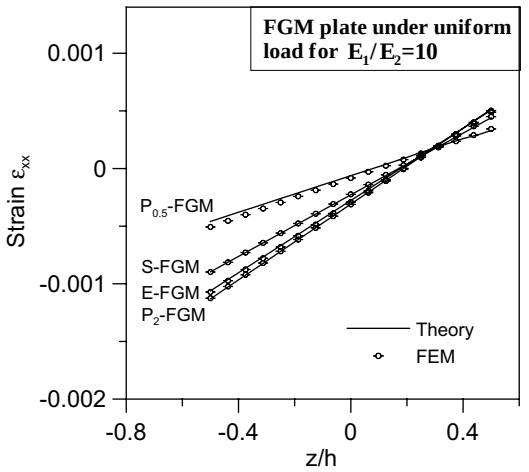

Fig. 24. The comparison of the strains ε_{xx} at the center of $P_{0.5}$-FGM, S-FGM, E-FGM, and P_2-FGM plates for $E_1/E_2 = 10$.

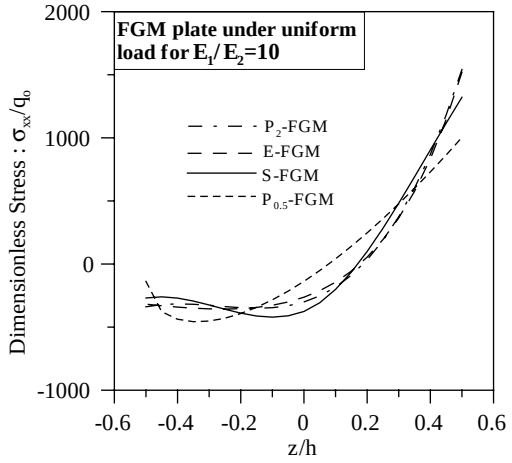

Fig. 25. The comparison of the stresses σ_{xx} at the center of $P_{0.5}$-FGM, S-FGM, E-FGM, and P_2-FGM plates for $E_1/E_2 = 10$.

4. Conclusion

In this study, the authors derive the theoretical solutions of FGM plates under transverse loads by Fourier series expansion. The theoretical results are also checked by finite element analysis. The results lead to the following conclusions:

(1) The closed-form solutions of the deflection, strain, stress, moment of an FGM plate with the material properties of $E = E(z)$ only have been derived based on the medium-thick plate assumption, and are functions of Q_{11} and S_{11} which can be easily obtained by integrating the material properties along the thickness. These formulations are also applicable to the homogeneous plates by letting the Young's modulus be a constant.

(2) Under the assumption of medium-thick plate in which the thickness h is in the range $\frac{1}{20}-\frac{1}{100}$ of its span approximately, the theoretical results, by Fourier series expansion, of the rectangular simply-supported FGM plates subjected to transverse loads agree very well with those of finite element analysis.
(3) The effect of changing Poisson's ratio on the mechanical behavior of the FGM plates is very small. Therefore the Poisson's ratios of FGM plates can be assumed to be constant.
(4) The neutral surface of the FGM plates depends on the variation of material properties in the thickness direction, or the ratio of E_1/E_2 for certain material distribution. While the location of the neutral surface is independent of the aspect ratio, or the external loads.
(5) The stresses of the FGM plates along the thickness direction are not linearly proportional to z, however, it is a function $z \cdot E(z)$. For the numerical study, the Young's moduli of the FGM plates are functions of z of order 2, therefore the stress represents a function of z of order 3.
(6) The maximum tensile stress of the FGM plates is located at the bottom surface of the plate. This phenomenon is the same as that of a homogeneous plate. However, the maximum compressive stress moves to the inner side of the plate, rather than at the top surface of the FGM plate.